

# Radiation Hardness Tests of SiPMs for the JLab Hall D Barrel Calorimeter<sup>☆</sup>

Yi Qiang<sup>a,\*</sup>, Carl Zorn<sup>a</sup>, Fernando Barbosa<sup>a</sup>, Elton Smith<sup>a</sup>

<sup>a</sup>Jefferson Lab, 12000 Jefferson Ave, Newport News, VA 23606

## Abstract

We report on the measurement of the neutron radiation hardness of silicon photomultipliers (SiPMs) manufactured by Hamamatsu Corporation in Japan and SensL in Ireland. Samples from both companies were irradiated by neutrons created by a 1 GeV electron beam hitting a thin lead target at Jefferson Lab Hall A. More tests regarding the temperature dependence of the neutron radiation damage and self-annealing were performed on Hamamatsu SiPMs using a calibrated Am-Be neutron source from the Jefferson Lab Radiation Control group. As the result of irradiation both dark current and dark rate increase linearly as a function of the 1 MeV equivalent neutron fluence and a temperature dependent self-annealing effect is observed.

**Keywords:** Silicon photomultiplier, SiPM, MPPC, Radiation damage, Barrel Calorimeter

## 1. Introduction

A Silicon photomultiplier (SiPM) is a photon-counting device consisting of multiple avalanche photodiode (APD) pixels operating in Geiger mode. It is also known as Multi-Pixel Photon Counter (MPPC). Each APD pixel of the SiPM outputs a pulse signal when it detects photons and the signal output from the SiPM is the total sum of the signals from all APD pixels. The SiPM offers the high performance needed in photon counting and is used in diverse applications for detecting extremely weak light intensities at the photon-counting level.

For Hall D At Jefferson Lab [1], we investigated the use of SiPMs to collect light from the Barrel Calorimeter. One of the requirements for such devices is sufficient radiation hardness to withstand many years of operation. As the neutron background is expected to be the major source of radiation damage in the Hall <sup>1</sup>, we did a series of tests of the neutron radiation damage to SiPMs at various conditions to evaluate the life time of SiPMs in Hall D.

## 2. Radiation Damage in Silicon Detectors

The bulk damage in silicon detectors caused by hadrons or higher energy leptons and photons is primarily due to displacement of primary knock-on atoms from the lattice [2]. For neutrons or electrons with kinetic energy above 175 eV and

260 keV, respectively, they will start to generate Frenkel pairs (a pair of a silicon interstitial and a vacancy) along their tracks in silicon material. With higher energy, more than 35 keV for neutrons and 8 MeV for electrons, a dense cluster of defects will be formed at the end of the primary PKA track.

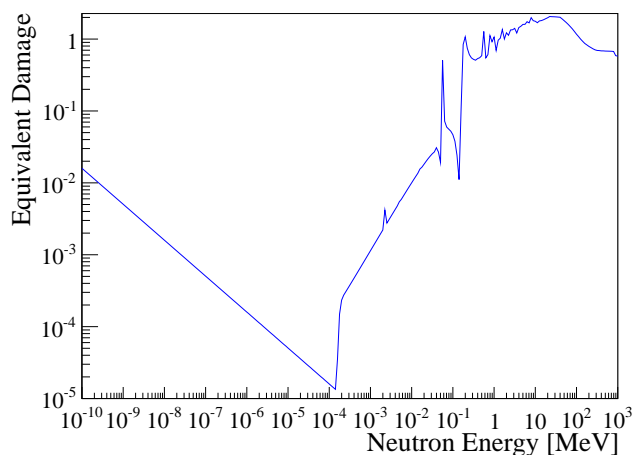


Figure 1: Effective damage to Silicon detectors relative to 1 MeV neutron. Data at different energy ranges are taken from References [3, 4, 5].

The defects will effect silicon detector's performance in various levels depending on their concentration, energy level and the respective electron and hole capture cross-section. For instance, defects with energy levels in the middle of the forbidden gap acting as recombination/generation centers are responsible for an increase of the reverse current. Interactions with dopants change the effective doping concentration and therefore change the operating voltage of the detector. Finally, defects acting as trapping centers reduce the charge collection efficiency.

The radiation damage of neutrons to Silicon detectors has been extensively summarized in the literature. In this paper, we

<sup>☆</sup> Authored by Jefferson Science Associates, LLC under U.S. DOE Contract No. DE-AC05-06OR23177. The U.S. Government retains a non-exclusive, paid-up, irrevocable, world-wide license to publish or reproduce this manuscript for U.S. Government purposes.

\*Corresponding author

Email address: yqiang@jlab.org (Yi Qiang)

<sup>1</sup> An early irradiation test on SiPMs using a series of high activity Cs-137 sources in Jefferson Lab showed that SiPMs are insensitive to electromagnetic radiation and there was no significant change in performance of SiPMs up to 2 krads of gamma irradiation.

40 took data from References [3, 4, 5] to convert the neutron flux  
 41 to the **1 MeV neutron fluence** based on the effective damage  
 42 caused by neutrons with different energies. The weight of such  
 43 a conversion is plotted in Fig. 1.

### 44 3. Test with Electron Beam

45 In addition to the goal of testing the neutron radiation damage  
 46 to SiPMs, we also confirmed our knowledge of the neutron  
 47 background.

#### 48 3.1. Test Setup

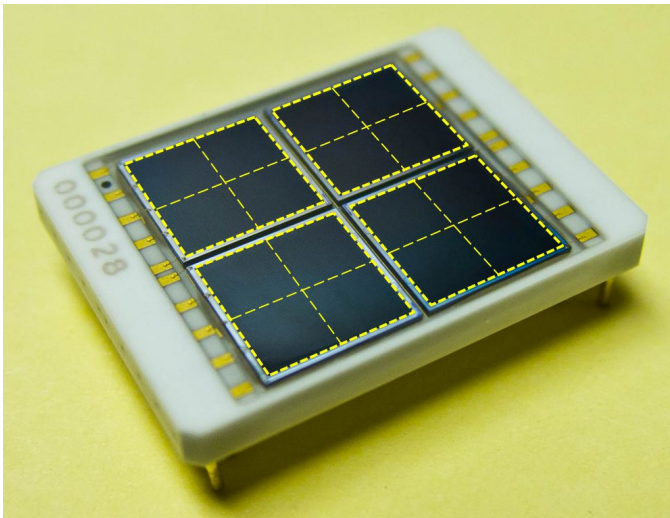


Figure 2: A  $4 \times 4$  SiPM array of  $3 \times 3$  mm SiPM cells from Hamamatsu and individual cells are marked by dashed lines.

49 The irradiation was carried out during the PRex experi-  
 50 ment [6] at Jefferson Lab Hall A, with a 1 GeV electron beam  
 51 incident on a 0.5 mm Pb target. During the two-day test, one  
 52 Hamamatsu unit<sup>2</sup> and one SensL unit<sup>3</sup> were irradiated. Both  
 53 units are  $4 \times 4$  arrays of  $3 \times 3$  mm<sup>2</sup> SiPMs and were powered  
 54 to a gain of  $0.75 \times 10^6$ . A photograph of the Hamamatsu SiPM  
 55 array is shown in Fig. 2.

56 Both SiPM units were placed inside a dark box together with  
 57 their pre-amplifiers. The light from a pulsed LED was guided  
 58 into the box through an optical fiber and then diffused by a  
 59 diffuser to provide uniform light on both units. The box was  
 60 positioned 20 meters away from the Hall A Pb target and 135  
 61 degrees backwards to the beam direction as illustrated in Fig. 3  
 62 to reduce the effect from other sources of radiation such as pho-  
 63 tons and charged particles. While the box had direct view of  
 64 the target, the rest of the equipment was shielded by a con-  
 65 crete wall. The shape of the output signals, including amplitude  
 66 and width, was continuously recorded by an oscilloscope. In

<sup>2</sup>A preproduction unit of S10943-0258(X) MPPC with  $50 \mu\text{m}$  pixels, equivalent to new S12045.

<sup>3</sup>A SPMArray unit based on ceramic design with  $35 \mu\text{m}$  pixels - Wafer Batch Code X4151-05 using SPM3035 design.

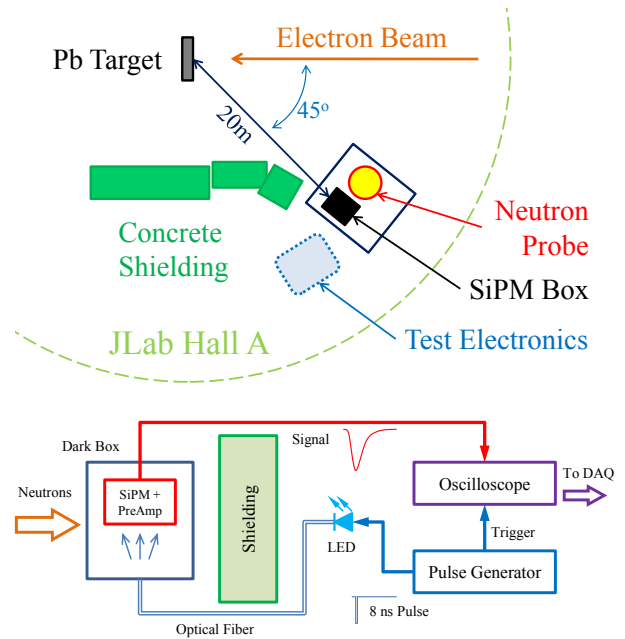


Figure 3: The floor plan and readout scheme for the SiPM radiation test in Hall A.

67 the middle of the irradiation period, the power supplies of both  
 68 SiPMs were turned off intentionally to see whether the power-  
 69 ing condition affects the radiation damage. After the irradiation,  
 70 both SiPMs were stored at room temperature, 20-25°C, for the  
 71 self-annealing test.

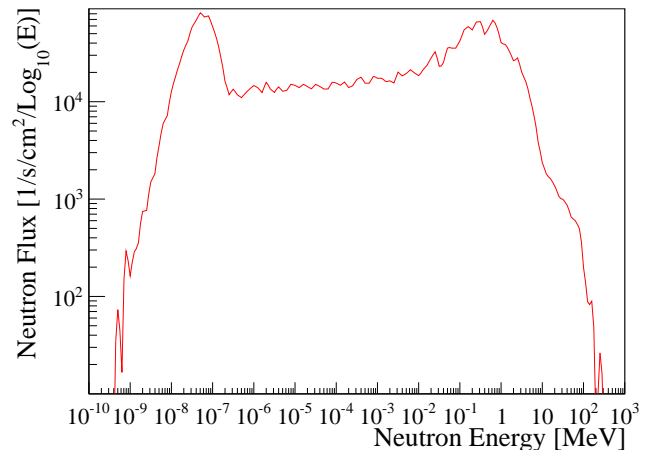


Figure 4: The simulated neutron energy spectrum at the SiPM testing area in Hall A with  $50 \mu\text{A}$  1 GeV electron on a 0.5 mm Pb target.

A  $\text{BF}_3$  neutron probe was positioned next to the dark box to monitor the relative change of the neutron flux in real time. In order to obtain the absolute reading of the effective 1 MeV neutron fluence, a couple of the same type of Hamamatsu SiPMs were later irradiated by a calibrated AmBe neutron source to a similar damage level. As the AmBe source has a well known

78 narrow energy spectrum peaking at about 4 MeV [7], its fluence  
 79 was calculated by convoluting the neutron flux spectrum with  
 80 the effective damage curve shown in Fig. 1. Then the fluence  
 81 in Hall A was calculated by comparing the damage the  
 82 SiPMs received in both cases.

83 As a result, we determined that the two SiPMs in Hall A re-  
 84 ceived a fluence of about  $3.7 \times 10^9$  n<sub>eq</sub>/cm<sup>2</sup>. The fluence mea-  
 85 surement also provides a good bench mark of our knowledge of  
 86 the radiation level in the experimental halls. The neutron flux in  
 87 Hall A was simulated in a GEANT3 framework customized to  
 88 the electron-beam environment [8, 9, 10]. The resulting energy  
 89 spectrum is shown in Fig. 4 and the fluence obtained from such  
 90 a simulation is consistent with the measured value within 50%.  
 91 The same code predicts that the  $3.7 \times 10^9$  n<sub>eq</sub>/cm<sup>2</sup> fluence will  
 92 be reached in about 13 years in Hall D with its high intensity  
 93 GlueX running <sup>4</sup> on a 30 cm liquid Hydrogen target.

### 94 3.2. Results

#### 95 3.2.1. Dark Current

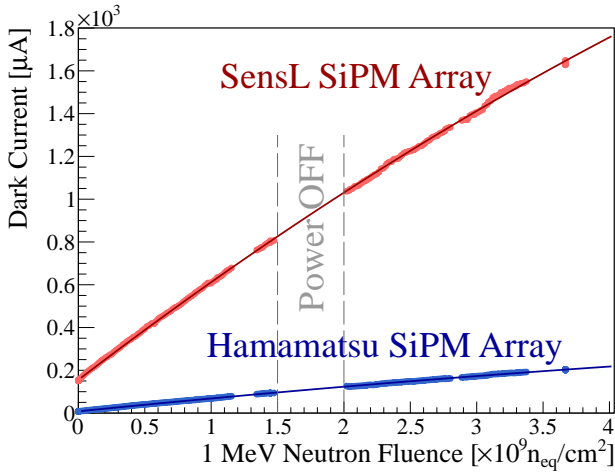


Figure 5: (Color online) The increase of the dark current of SiPMs as a function of the neutron fluence during the two-day irradiation in Hall A. The curves are fits using second order polynomials. The period with no data marked by grey dash lines corresponds to the time when the sensors were not powered, but continued to be irradiated.

96 The change of the SiPM dark current as a function of the ac-  
 97 cumulated neutron fluence is plotted in Fig. 5. As the beam was  
 98 turned on, the dark current of both SiPMs started to increase im-  
 99 mediately. By comparing the trends of the damage before and  
 100 after the period when the power was turned off, one can see  
 101 that the neutron damage remains the same no matter whether  
 102 the unit is powered or not. Over the course of the test, the dark  
 103 current increased by a factor of about 10 for the SensL SiPM  
 104 Array,  $160 \mu\text{A} \rightarrow 1.6 \text{ mA}$ , and 25 for the Hamamatsu SiPM  
 105 Array,  $8 \mu\text{A} \rightarrow 200 \mu\text{A}$ .

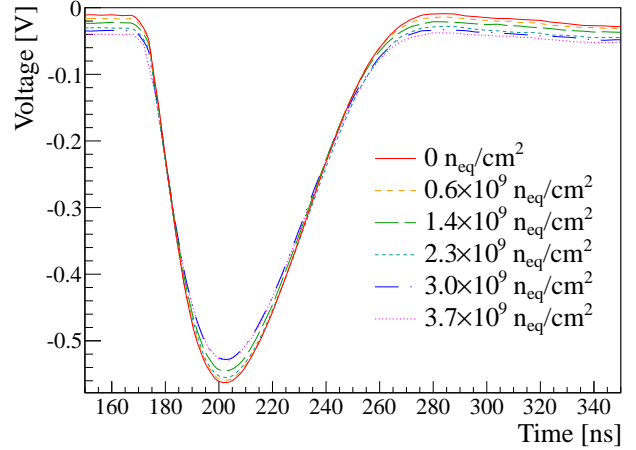


Figure 6: (Color online) Signals from the Hamamatsu SiPM array recorded by the oscilloscope during the irradiation.

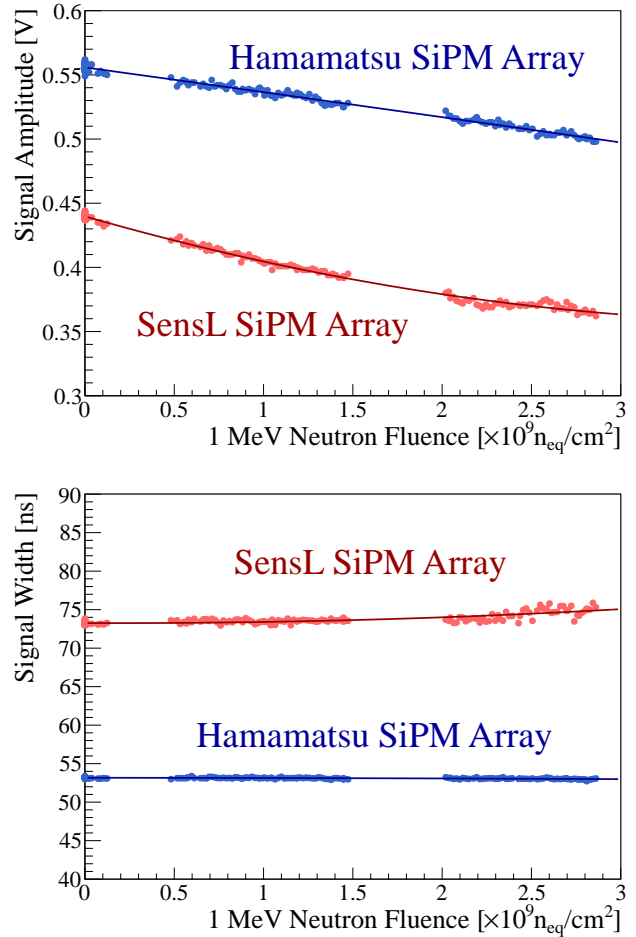


Figure 7: (Color online) The impact of neutron radiation damage on the signal shape, amplitude and width, of the SiPM output. The amplitude dropped slightly while no change was observed in the width. The curves are fits using second order polynomials.

### 3.2.2. Signal

The output signals from both SiPMs stayed relatively stable in contrast to the dramatic change of the dark current. The amplitude and width (50% to 50%) are plotted in Fig. 6 and 7. While the width shows no noticeable change, the amplitude dropped by about 10%.

### 3.2.3. I-V Curve

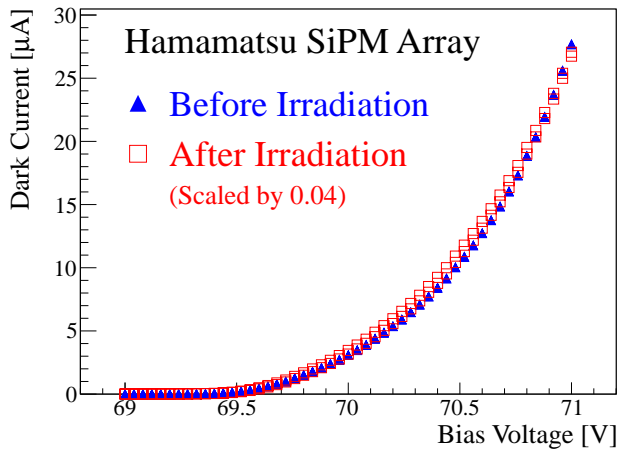


Figure 8: (Color online) The I-V curve of Hamamatsu SiPM array before and after the irradiation. The dark current after irradiation is scaled by a 0.04 for a better visual comparison and clearly the break down voltage was not effected by the neutron radiation.

The current vs. voltage (I-V) curves before and after irradiation are also compared for both units, and the comparison of the Hamamatsu SiPM array is shown in Fig. 8. Other than an overall change in scale, the I-V curves stay the same for both units and indicate that the break down voltage of the SiPM is not impacted by the neutron radiation.

### 3.2.4. Self-Annealing

Following the delivery of an intense prompt dose of radiation, one finds that not all damage to the lattice is permanent. So we studied the response of the sensors as they rested without further irradiation (self-annealing). The results of the self-annealing at room temperature after the prompt irradiation are plotted in Fig. 9 and 10. Both the dark current and signal amplitude recovered over time with a time constant close to 10 days. About half of the damage to the dark current recovered and the signal amplitude completely returned to the level before the irradiation.

## 4. Temperature Tests with a AmBe Neutron Source

The Hall A irradiation test revealed that the lifetime of the SiPM will be marginal in Hall D given the experimental requirement on the dark rate. Fortunately, a lower dark rate at

<sup>4</sup>Such a high intensity refers to a Bremsstrahlung photon flux of about 100 MHz/GeV close to the 12 GeV endpoint.

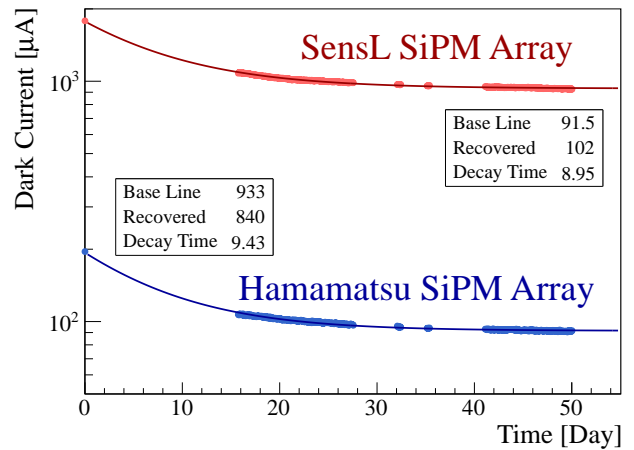


Figure 9: (Color online) The decline of dark current during SiPM's self-annealing at room temperature after the irradiation. The time constant for both samples is about 10 days and approximately half of the damage recovered. The data are fitted by an exponential function described in Eq. (1).

a fixed gain can be achieved if the SiPM is cooled. Cooling the SiPMs to 5°C will reduce the dark rate to about 1/3 compared with 20°C and will certainly allow more room for the increase of the dark rate caused by the neutron radiation damage. However, whether such a dependence will be effected by radiation damage was unknown, therefore a systematic study of the temperature dependence of the neutron radiation damage and annealing was performed using a calibrated AmBe neutron source.

### 4.1. Test Procedure

Twelve 1 × 1 mm<sup>2</sup> SiPM units from Hamamatsu with 50 μm pixels (PN# S10362-11-050C) were irradiated during this test.

Since the previous Hall A irradiation test shows no correlation between the damage and the powering condition, all the SiPMs were not powered during the irradiation or annealing except when their dark currents were measured. If not specifically mentioned, the dark current was always measured at room temperature regardless of the SiPM's irradiation or annealing temperatures. This allows direct comparison of results between samples regardless of the temperature at which they were irradiated or annealed. It is assumed that taking the test samples to room temperature during the short time of the measurement does not significantly influence the results. The unit was then powered off and put back to its previous temperature after the dark current was measured. All the SiPMs were powered to a gain of 0.84 × 10<sup>6</sup> during the dark current measurements. The gain was determined using the ADC spectra and more details can be found in Sec. 4.2.2.

The test consists of the following steps as shown in Fig. 11:

1. In the first stage, six units were irradiated at -5°C while the remaining six units were irradiated at room temperature, ~ 25°C. The irradiation lasted four days and the total fluence each unit received was about 1.4 × 10<sup>9</sup> n<sub>eq</sub>/cm<sup>2</sup>.

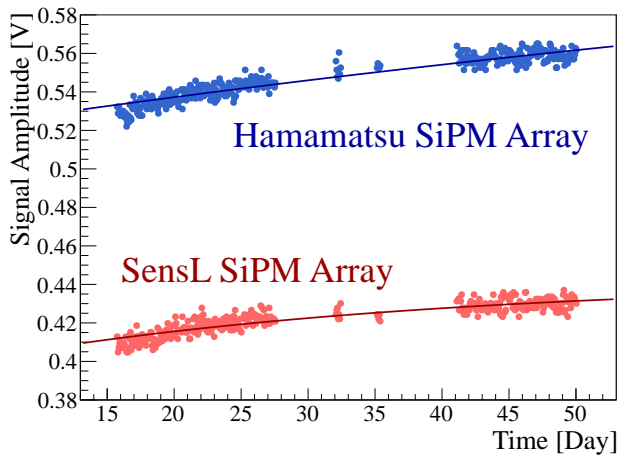


Figure 10: (Color online) The recovery of the signal amplitude. Signals from both samples returned to their levels before neutron irradiation.

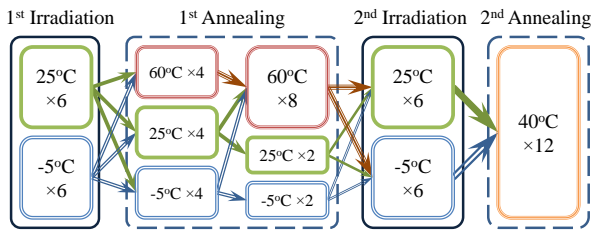


Figure 11: (Color online) Steps of the irradiation/annealing temperature dependence test. Numbers in boxes indicate number of samples tested in each group.

2. Right after the first irradiation, all the units were immediately stored at three different temperatures,  $-5^{\circ}\text{C}$ ,  $25^{\circ}\text{C}$  and  $60^{\circ}\text{C}$ , for their first annealing. Every group had two units from each temperature group of the first irradiation. With all the units annealed, half of the units from the  $-5^{\circ}\text{C}$  and  $25^{\circ}\text{C}$  annealing groups were further heated to  $60^{\circ}\text{C}$  to investigate any additional recovery while the rest of the units were still kept at their original temperatures.
3. After the first annealing was completed, all the units were irradiated again at  $-5^{\circ}\text{C}$  or  $25^{\circ}\text{C}$  for four more days with an additional fluence of  $1.7 \times 10^9 \text{ n}_{\text{eq}}/\text{cm}^2$ , to see whether the radiation damage due to the first irradiation would effect the subsequent damage rate.
4. At the end, all the units were heated to  $40^{\circ}\text{C}$  for a final accelerated annealing.

## 4.2. Results

### 4.2.1. Temperature Dependence of Radiation Damage and Recovery

The average current of all units before the irradiation test is  $86 \pm 3 \text{ nA}$  and the uncertainty is the standard deviation of the measurements of individual units. After the first irradiation, the average current of the group at  $-5^{\circ}\text{C}$  increased to  $771 \pm 66 \text{ nA}$ , and for the  $25^{\circ}\text{C}$  group, the current went up to  $660 \pm 38 \text{ nA}$ .

Such a  $110 \text{ nA}$  difference suggests two possibilities, one is a temperature dependence of the radiation damage and the other one is a temperature dependence of the damage recovery.

For the units annealed at  $60^{\circ}\text{C}$  during the first annealing, the average dark currents of the units from the  $-5^{\circ}\text{C}$  and  $25^{\circ}\text{C}$  irradiation groups dropped to  $365 \pm 61 \text{ nA}$  and  $341 \pm 23 \text{ nA}$ , respectively. The consistency of these two values excludes the temperature dependence of the radiation damage to the limit of the variation among samples.

On the other hand, if the recovery at  $-5^{\circ}\text{C}$  is much weaker or slower than  $25^{\circ}\text{C}$ , the recovery during the four days of irradiation will reduce the damage to the  $25^{\circ}\text{C}$  group more. The results of the annealing at different temperatures indeed confirm this hypothesis and the recovery at higher temperature is faster and stronger.

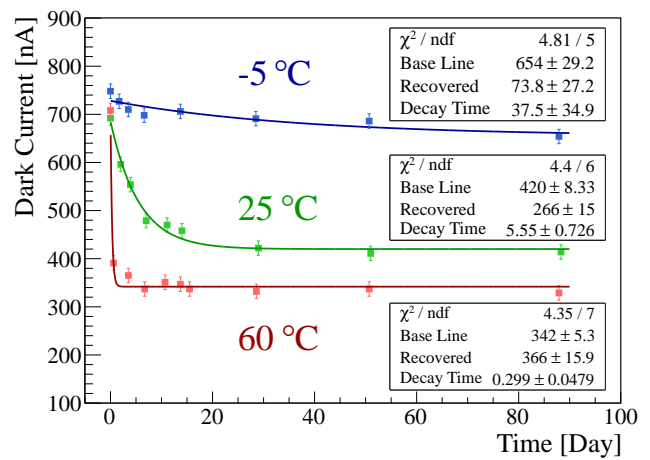


Figure 12: (Color online) The recovery of the dark current at different temperatures after the first irradiation. All the values were measured at  $25^{\circ}\text{C}$  and the uncertainties only include the accuracy of the measurements.

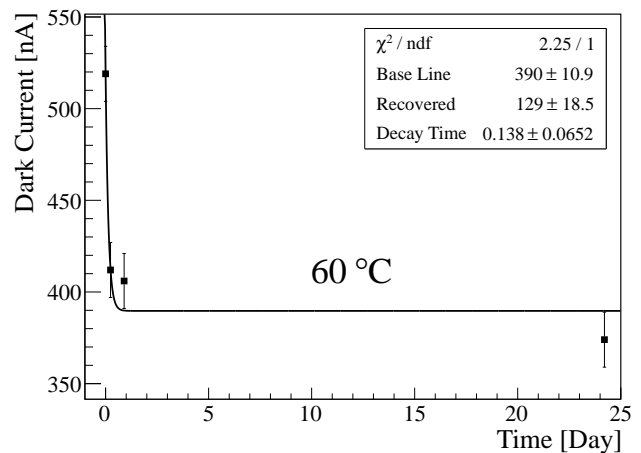


Figure 13: The secondary recovery at  $60^{\circ}\text{C}$  at the end of the first annealing of selected units previously annealed at  $-5^{\circ}\text{C}$  or  $25^{\circ}\text{C}$ .

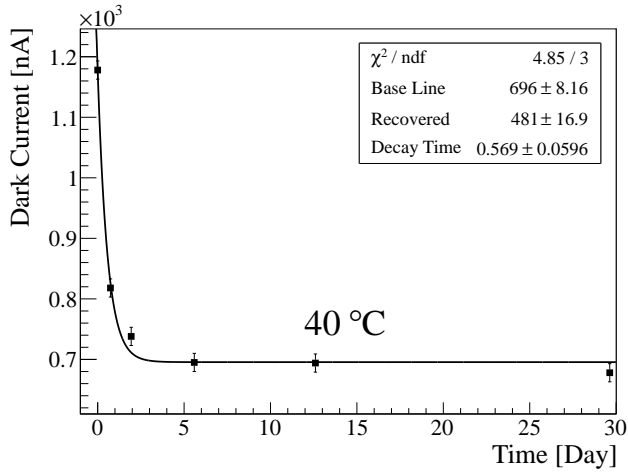


Figure 14: The final recovery of SiPMs at 40°C after the second irradiation.

The recovery curves at various temperatures are shown in Fig. 12, 13 and 14. The uncertainties in these plots only include the estimated uncertainty of the current measurement, 15 nA, while the variation among individual units is not included since it has no impact on the fit of the recovery time constant. The data are fitted with a simple exponential decay function with a constant baseline offset:

$$I = b + a \cdot e^{-t/\tau} \quad (1)$$

where  $b$  is the baseline dark current after annealing,  $a$  is the recoverable damage and  $\tau$  is the time constant.

Fig. 12 shows the recovery of the SiPM dark current at  $-5^\circ\text{C}$ ,  $25^\circ\text{C}$  and  $60^\circ\text{C}$  right after the first irradiation. It is very clear that the units annealed at higher temperature recover faster and reach a lower asymptotic dark current. In order to see whether the baseline will be fixed after first annealing at a lower temperature, half of the units from the groups of  $-5^\circ\text{C}$  and  $25^\circ\text{C}$  were heated to  $60^\circ\text{C}$  for a secondary annealing. As shown in Fig. 13, additional recovery was observed and the time constant is consistent with the one obtained from the original  $60^\circ\text{C}$  group. The time constant of  $40^\circ\text{C}$  annealing were measured later after the second irradiation, as shown in Fig. 14.

The temperature dependence of the recovery time constants can be described by an exponential curve

$$\tau(T) = 41 \cdot e^{-0.10 \cdot T} \text{ day} \quad (2)$$

as plotted in Fig. 15.

Fig. 16 shows the temperature dependence of the baseline. The uncertainties in the plot now include the variations from individual units. Given the limited accuracy and the number of data points, the function of the temperature dependence cannot be well determined. It is clear nevertheless that when the annealing temperature is above  $40^\circ\text{C}$ , the change of the baseline can not be clearly identified given the variation of individual units.

As already discussed, the damage will further recover if higher temperature is applied later. In order to see whether the

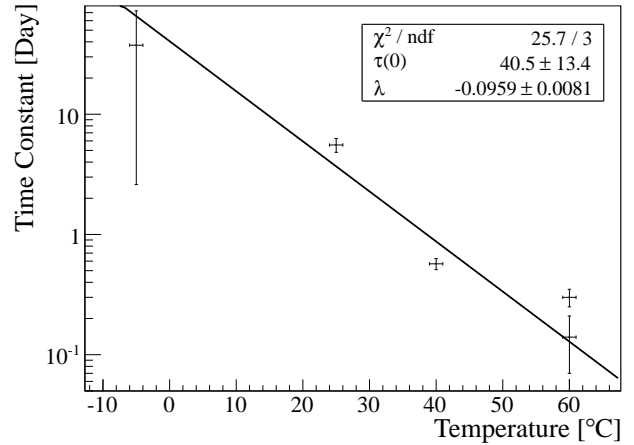


Figure 15: The dependence of the time constant  $\tau$  in Eq. (1) of the annealing on the temperature. Such a dependence is fitted by an exponential curve.

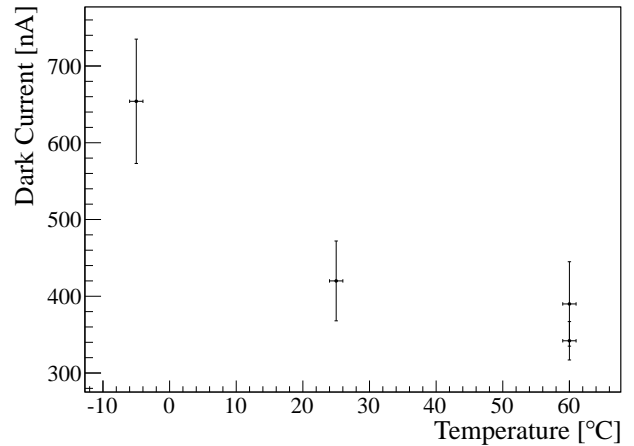


Figure 16: The dependence of the baseline  $b$  in Eq. (1) of the annealing on the temperature.

recovery would reverse when the annealed units are stored at a lower temperature, half of the units annealed at  $60^\circ\text{C}$  were put into a freezer for several weeks, and no indication of any increase in the dark current was found.

The two units which were always kept at  $-5^\circ\text{C}$  during the annealing after the first irradiation were annealed at  $40^\circ\text{C}$  with the rest of the units after the second irradiation. At the end, both units recovered to a level consistent with all the other units. This fact suggests that the temporary damage resulting from previous irradiations can always be recovered with sufficiently high annealing temperature.

Finally, we plot the average dark current with annealing at temperature above  $40^\circ\text{C}$  as a function of neutron fluence in Fig. 17. The error bars represent the variation of dark current among units. The slopes of the damage during the two irradiations are consistent and it is clear that the previous irradiation will not effect later ones.

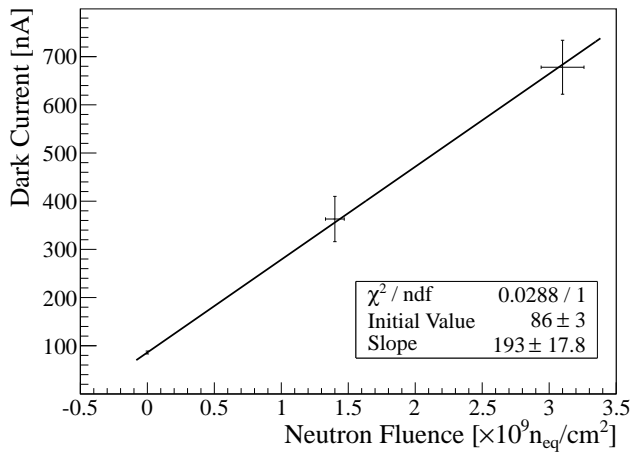


Figure 17: Damage curve of 1 mm SiPM as a function of 1 MeV neutron fluence assuming annealing at 40-60°C. The current was measured at 25°C with a gain of  $0.84 \times 10^6$ .

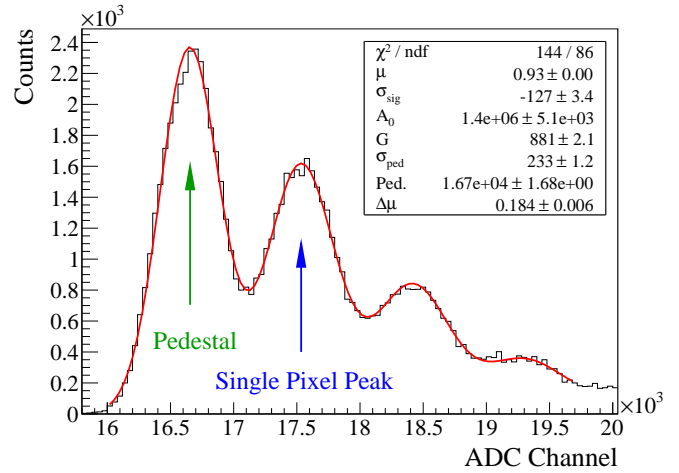


Figure 18: A typical ADC spectrum for the dark rate measurement. The data were taken from SiPM #1854 at 25°C after the first irradiation. The description of the fitting function can be found in the text.

#### 4.2.2. Relation between Dark Rate and Dark Current and Their Temperature Dependence

What was being measured all the time is the dark current, but it is the dark rate which actually affects the performance of the Barrel Calorimeter in Hall D. In order to measure the dark rate, a DAQ system using a gated ADC was set up to record the random dark pulses generated by SiPMs. The length of the gate is chosen to be 200 ns which is longer than the pulse width of SiPMs,  $\sim 80$  ns from 10% to 10%. Three  $1 \times 1$  mm<sup>2</sup> SiPMs were measured at various temperatures between  $-5^\circ\text{C}$  and  $25^\circ\text{C}$  while the gain was kept constant by adjusting the bias voltage based on the characteristic curve provided by Hamamatsu [11]. In other words, the voltage setting above breakdown or over-bias was kept constant. All three units were also part of the irradiation test therefore their ADC spectra after the irradiation were also taken for comparison.

Fig. 18 shows a typical ADC spectrum from a  $1 \times 1$  mm<sup>2</sup> SiPM. The histogram was fitted by a convolution of a discrete distribution function and a gaussian function.

$$A(x) = A_0 \cdot P(n|\mu, \Delta\mu) \otimes \text{Gaus}(x|n \cdot G + \text{ped}, \sigma_n) \quad (3)$$

where  $A_0$  is the normalization factor. The discrete distribution,  $P(n|\mu, \Delta\mu)$ , represents the probability that the number of pixels fired is equal to  $n$ , and it contains two Poisson distributions with one for the primary pixels fired and the other for the total of cross talk or after pulses [12] caused by the primary pixel:

$$\begin{aligned} P(n|\mu, \Delta\mu) &= \sum_{n=i+j} \text{Pois}(i|\mu) \cdot \text{Pois}(j|i \cdot \Delta\mu) \\ &= \sum_{n=i+j} \frac{e^{-(\mu+i\Delta\mu)} \mu^i (i\Delta\mu)^j}{i! j!} \end{aligned} \quad (4)$$

where  $\mu$  is the average number of primary pixels fired and  $\Delta\mu$  is the average number of pixels fired around the primary pixel due

to cross talk and after pulses. The Gaussian function,  $\text{Gaus}(x|n \cdot G + \text{ped}, \sigma_n)$ , represents the distribution of the charge with the number of pixels fired equal to  $n$ .  $G$  is the total gain<sup>6</sup> in ADC channels and  $\text{ped}$  is the ADC pedestal value. The width,  $\sigma_n$ , is equal to

$$\sigma_n = \sqrt{\sigma_{\text{ped}}^2 + n \cdot \sigma_{\text{sig}}^2} \quad (5)$$

where  $\sigma_{\text{ped}}$  is the width of the pedestal and  $\sigma_{\text{sig}}$  is the intrinsic width of a single pixel signal. Such a function is valid when both the signal occupancy and the  $\Delta\mu$  are small, which is true for our test condition. Otherwise, the function needs to be modified by replacing the Poisson distributions with binomial distributions.

The absolute gain of SiPMs was calculated by dividing the total gain  $G$  by the known ADC conversion factor and the gain of the preamplifiers. As shown in Fig. 19, the gain is relatively stable at different temperatures as long as the bias voltage setting was adjusted to compensate for the change in the breakdown voltage with temperature to have a fixed over-bias. The uncertainties shown in the plot only include the statistical uncertainty from the fit and the uncertainty of the temperature reading. However, due to the temperature gradient in the cooling device, the gain fluctuates slightly around the average value,  $0.84 \times 10^6$ .

Fig. 20 shows the correlation between the dark current and the dark rate, and the dark current has been corrected for the deviation of the gain to the average value. The correlation is well described by a linear function:

$$I = 0.190 \text{ nA/kHz} \cdot f + 3.84 \text{ nA} \quad (6)$$

The slope corresponds to an average gain of  $1.19 \times 10^6$  which is about 42% higher than the actual gain. Part of the mismatch comes from the cross talk and after pulses which are

<sup>5</sup>Their serial numbers are 1853, 1854 and 1855.

<sup>6</sup>It includes the intrinsic gain of an APD pixel, the gain of the pre-amplifiers and the ADC's analog-to-digital conversion factor.

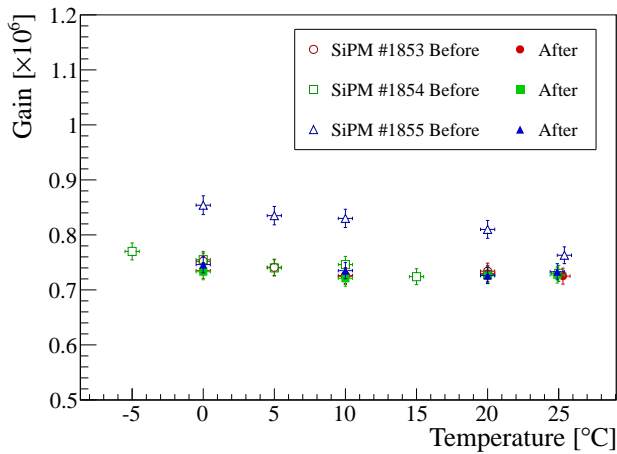


Figure 19: The absolute gain of SiPMs at different temperatures at constant over-bias. Different legends represent the data from different units before and after the irradiation.

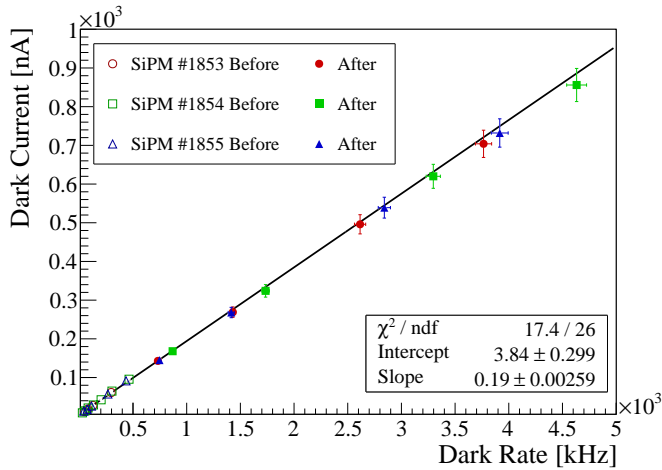


Figure 20: The correlation between the dark current and dark rate with a gain of  $0.84 \times 10^6$ .

not counted in the extraction of the dark rate. The rest may be attributed to the fact that Eqn. (3) does not fully account for the pulses partially integrated in the ADC gate<sup>7</sup>. Clearly, the radiation damage does not have any impact on this relation.

On the other hand, there is no significant temperature dependence of the cross talk and after pulses observed as shown in Fig. 21. And the radiation damage doesn't change them as well.

Fig. 22 shows the temperature dependence of the dark rate before and after the neutron irradiation. The dependence is exponential in the measured temperature range and the change of the temperature coefficient caused by the radiation damage is

<sup>7</sup>In retrospect, we realize that a longer gate width may have allowed a more accurate determination of the extracted dark rate from the fit.

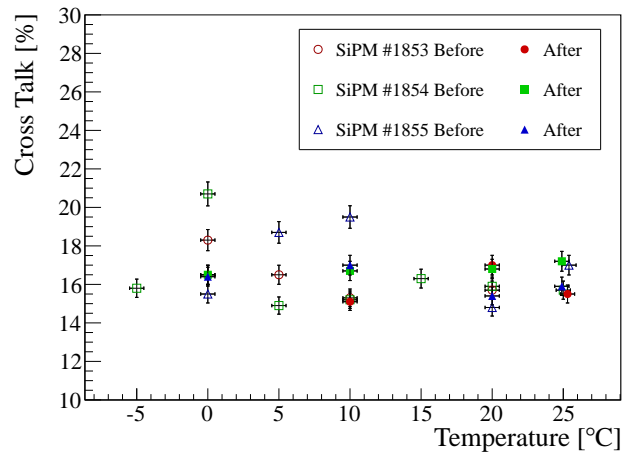


Figure 21: The dependence of cross talk on temperature.

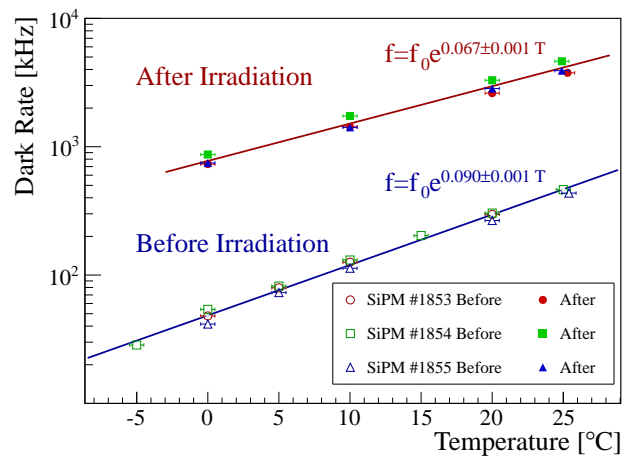


Figure 22: The dependence of the dark rate before and after irradiation on temperature.

relatively small. As a result, the average dependence is

$$f = f_0 \cdot e^{0.075 \cdot (T - T_0)} \quad (7)$$

Such a behavior provides the motivation to cool SiPMs during beam time in Hall D to reduce the dark rate.

## 5. Summary

We measured the neutron radiation damage to SiPMs using neutrons generated by an electron beam at Jefferson Lab and a AmBe neutron source. We further studied the temperature dependence of the radiation damage and other properties including dark rate, dark current and damage recovery. We found that both dark rate and dark current increase linearly as a function of the total neutron fluence and the damage does not depend on the temperature or operating voltage. Part of the acute damage will recover. The speed and the extent of this annealing process



307 strongly depends on the temperature and is faster and stronger  
308 at higher temperature. Increasing the temperature of a dam-  
309 aged unit previously annealed at a certain temperature brings  
310 further recovery, but lowering the temperature will not reverse  
311 the recovery achieved. We also measured the temperature de-  
312 pendence of the dark current and dark rate of SiPMs at a fixed  
313 gain. Such a dependence is not strongly affected by the neutron  
314 radiation damage.

315 The results obtained by this study provided important infor-  
316 mation for implementing SiPMs as the readout of the Barrel  
317 Calorimeter in JLab Hall D.

## 318 6. Acknowledgement

319 We acknowledge the JLab Hall A staff for their support dur-  
320 ing the electron beam irradiation test. We acknowledge M.  
321 Washington, J. Jefferson and D. Hamlette from the JLab Rad-  
322 Con group for providing AmBe source and calibrated neutron  
323 probes. We also acknowledge Dr. P. Degtyarenko from the  
324 JLab RadCon group for calculating the neutron dose in Hall A.  
325 This work was supported by the U.S. Department of Energy.  
326 Jefferson Science Associates, LLC, operates Jefferson Lab for  
327 the U.S. DOE under U.S. DOE contract DE-AC05-06OR23177.

## 328 References

- 329 [1] <http://www.jlab.org/Hall-D>.
- 330 [2] G. Lindstrom, Radiation damage in silicon detectors, Nucl. Instrum.  
331 Meth. A512 (2003) 30–43. doi:10.1016/S0168-9002(03)01874-6.
- 332 [3] P. J. Griffin, J. G. Kelly, T. F. Luera, J. VanDenburg, SNL RML Recom-  
333 mended Dosimetry Cross Section Compendium, Sandia Nat. Lab Report  
334 SAND92-0094.
- 335 [4] A. Konobeyev, Y. Korovin, V. Sosnin, Neutron displacement  
336 cross-sections for structural materials below 800 mev, Jour-  
337 nal of Nuclear Materials 186 (2) (1992) 117 – 130. doi:DOI:  
338 10.1016/0022-3115(92)90328-I.  
339 URL [http://www.sciencedirect.com/science/article/pii/  
340 002231159290328I](http://www.sciencedirect.com/science/article/pii/S002231159290328I)
- 341 [5] M. Huhtinen, P. A. Aarnio, Pion induced displacement damage in silicon  
342 devices, Nucl. Instrum. Meth. A335 (1993) 580–582. doi:10.1016/  
343 0168-9002(93)91246-J.
- 344 [6] JLab Experiment E06-002: The Lead Radius Experiment, Spokenper-  
345 sons: K. Kumar, P. Souder, R. Michaels, K. Paschke, G. Urciuoli (2006).
- 346 [7] H. R. Vega-Carrillo, E. Manzanares-Acua, A. M. Becerra-Ferreiro,  
347 A. Carrillo-Nuez, Neutron and gamma-ray spectra of  $^{239}\text{Pu}$  and  
348  $^{241}\text{Am}$ , Applied Radiation and Isotopes 57 (2) (2002) 167 – 170.  
349 doi:10.1016/S0969-8043(02)00083-0.  
350 URL [http://www.sciencedirect.com/science/article/  
351 B6TJ0-45CN5MW-2/2/7f2e22e6d987ee8aea34a033075e5ca5](http://www.sciencedirect.com/science/article/B6TJ0-45CN5MW-2/2/7f2e22e6d987ee8aea34a033075e5ca5)
- 352 [8] P. V. Degtyarenko, M. V. Kossov, H. P. Wellisch, Chiral invariant phase  
353 space event generator. I: Nucleon antinucleon annihilation at rest, Eur.  
354 Phys. J. A8 (2000) 217–222. doi:10.1007/s100500070108.
- 355 [9] P. V. Degtyarenko, M. V. Kossov, H. P. Wellisch, Chiral invariant phase  
356 space event generator. II: Nuclear pion capture at rest and photonuclear  
357 reactions below the  $\Delta(3,3)$  resonance, Eur. Phys. J. A9 (2000) 411–  
358 420. doi:10.1007/s100500070025.
- 359 [10] P. V. Degtyarenko, M. V. Kossov, H. P. Wellisch, Chiral invariant phase  
360 space event generator. III: Modeling of real and virtual photon interac-  
361 tions with nuclei below pion production threshold, Eur. Phys. J. A9 (2000)  
362 421–424. doi:10.1007/s100500070026.
- 363 [11] Hamamatsu Corporation, MPPC S10362-11-050C Datasheet (2008).  
364 URL [http://sales.hamamatsu.com/assets/pdf/parts\\_S/  
365 mppc\\_kapd0002e08.pdf](http://sales.hamamatsu.com/assets/pdf/parts_S/mppc_kapd0002e08.pdf)
- 366 [12] D. Renker, E. Lorenz, Advances in solid state photon detectors, JINST 4  
367 (2009) P04004. doi:10.1088/1748-0221/4/04/P04004.